2.2 Strong Ground Motion

2.2.1 Strong Ground Motion Network

The world densest digital strong ground motion network of Taiwan with the station mesh of 3 km in the urban areas (Shin et al., 2000) monitored the strong ground motion of the 1999 Chi-Chi earthquake. Since 1996 the Seismological Center of the Central Weather Bureau (CWB) of Taiwan has been deploying over 600 seismometers, mostly strong ground motion instruments especially for the metropolitan areas, due to six-year Taiwan Strong Ground Motion Instrumentation Program (TSMIP). Over 400 free-field three-component acceleration records from the main shock were retrieved by 7 November 1999, especially from near-source stations.

The acceleration sensors used, have a flat response from DC to 50 Hz with a 200 samples per second and full scaling capacity of ± 2 g. The accelerographs are operated in trigger mode with the 20-seconds pre-event memory and 5-seconds post-event memory after the signal drops below the threshold level (Shin et al., 2000; Loh et al., 2000). Figure 2.2.1 shows the locations of the CWB free-field accelerograph stations and the epicenter of the main shock of the Chi-Chi earthquake.

2.2.2 Strong Motion Indices

In order to investigate the strong motion characteristics of the 1999 Chi-Chi earthquake, the Japan Meteorological Agency (JMA) instrumental seismic intensity (I_{JMA}), as well as other ground motion indices such as Spectrum Intensity (*SI*), Peak Ground Acceleration (*PGA*), and Peak Ground Velocity (*PGV*), were calculated. Four hundred twenty (420) free-field three-component acceleration records, which were retrieved from the CD-ROM of free-field strong-ground data (the Seismological Center of CWB, 1999), were used. The calculated indices are listed in the Appendix.

Since some of the near-fault ground motions are characterized by long-period, pulse-like time histories, an appropriate baseline correction scheme was used to preserve these important near-field motion characteristics. In this study, for the original acceleration records from the near-fault stations, the segmented base-line correction scheme, which adjusts the records by shifting the last part of zero-

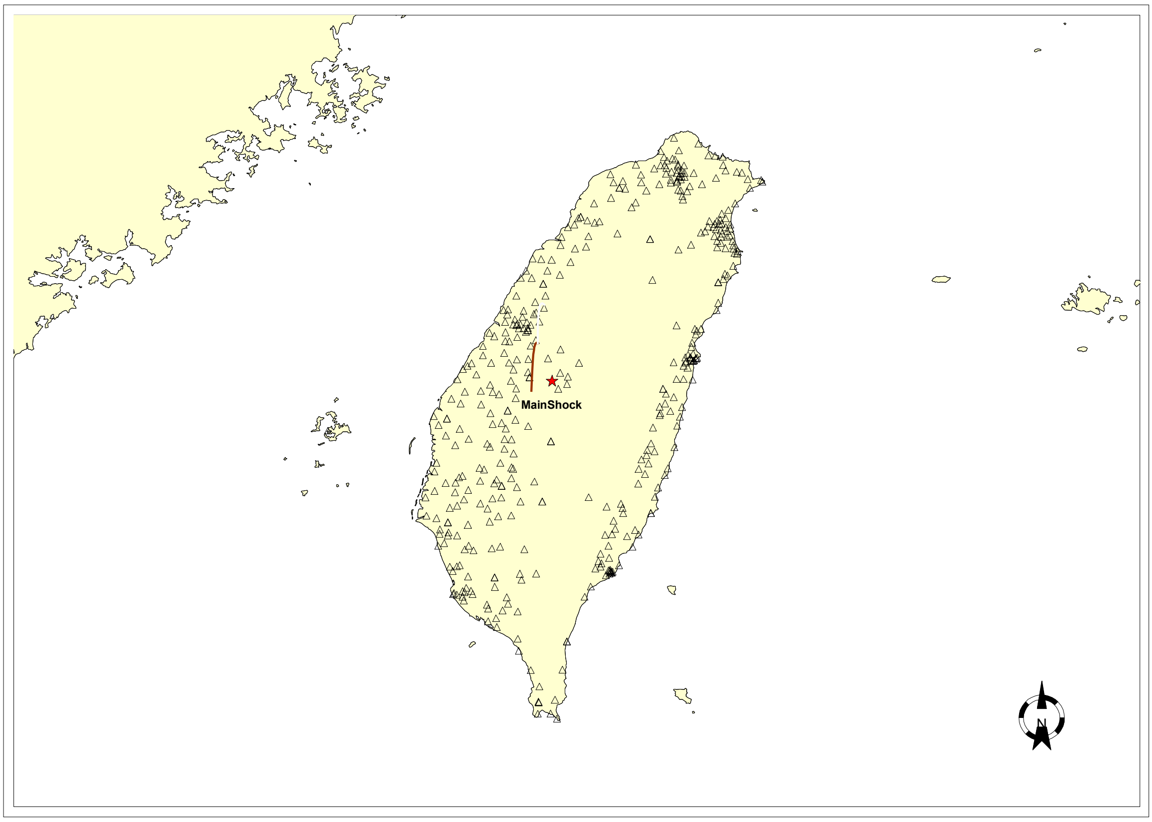

Figure 2.2.1. Locations of the CWB free-field strong motion stations, the epicenter, and the surface fault of the 1999 Chi-Chi, Taiwan earthquake.

lines, were applied (Boore, 1999; Kostadinov and Yamazaki, 2000). For the other stations, the average baseline correction was employed.

The velocity time histories were obtained by the ordinary differential equations applying to algebraic ones called Runge-Kutta tequnique and Newmark method for the near-fault stations and other stations, respectively.

At TCU052 and TCU068 stations in the northeast hanging-wall side of Chelungpu fault, the PGV reached as large as 266 cm/s and 384 cm/s, respectively. In contrary, at TCU129 station in the southern footwall side of the fault, the PGV observed as 79 cm/s, while its PGA reached more than 980 cm/s^2. This also can be seen in Figure 2.2.2, which shows the distribution of the resultants PGV and PGA. In spite of these large PGV values, structural damages around the instruments were not so severe. This is due to the fact that the period of the pulse is too long at these stations. Since the PGV is affected by such a long period content, it is sometimes not a reliable parameter to express structure damages.

Instrumental Seismic Intensity

In Japan, the JMA intensity has been used as a measure of strong shaking for many years. It had been determined by the human judgment of JMA officers. But, in the early 90s, JMA started to move to an instrumental seismic intensity from human judgment. On 1996, the JMA intensity scale was revised and a large number of seismometers measuring the JMA intensity were deployed throughout in Japan (JMA, 1996). The instrumental seismic intensity, which is obtained from the three-component of acceleration records, is currently broadcasted through public TVs and radios soon after the occurrence of earthquakes. For disaster management agencies in Japan, it is used as the most important index to estimate structural damage due to earthquakes (Yamazaki, 1998). The details of JMA seismic intensity algorithms are given in Shabestari and Yamazaki (1998).

In Taiwan, however, the old JMA intensity scale determined by human judgment is still used. An intensity distribution presented by CWB was made using an attenuation relation for PGA and

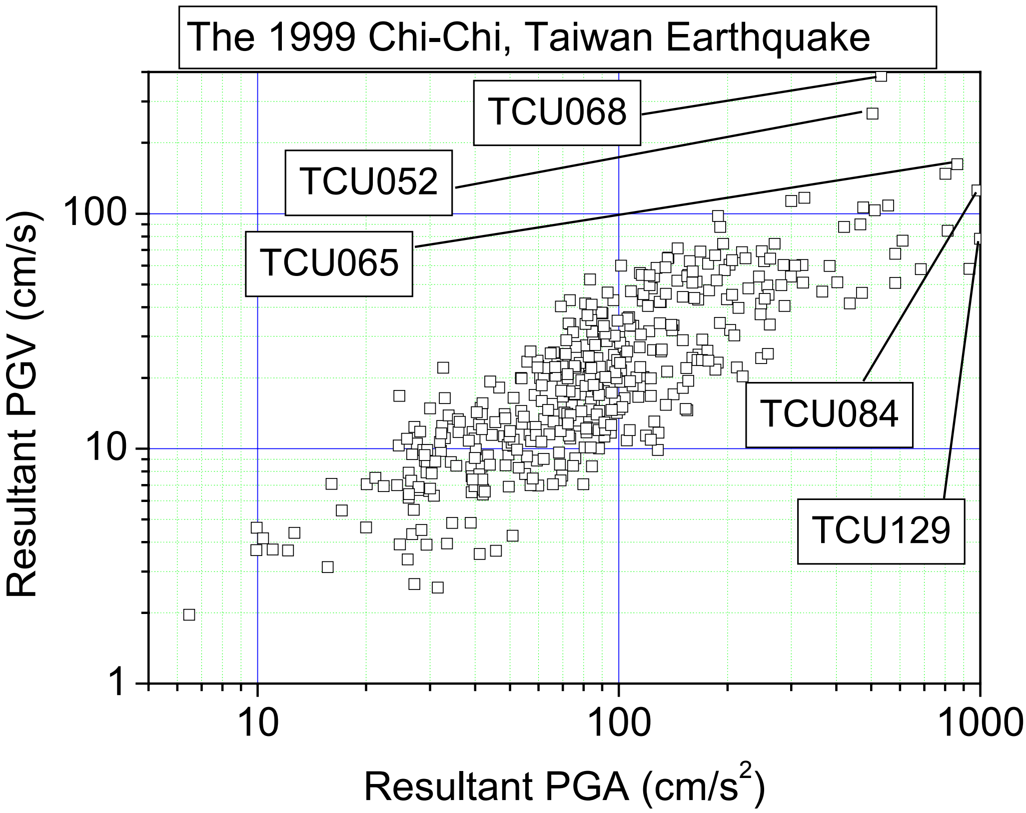

Figure 2.2.2. The relation between resultants PGV and PGA for the 1999 Chi-Chi, Taiwan earthquake.

Kawasumi equation. Kawasumi equation, which relates the PGA and the old JMA intensity scale, was proposed in 1943. But, due to the recent advancement in the sensitivity of accelerometers, the Kawasumi equation was found not to fit the PGA- instrumental JMA intensity relation (Tong and Yamazaki, 1996).

Figure 2.2.3 shows the distribution of the instrumental seismic intensities (I_{JMA}), calculated from the 420 CWB stations. It is seen that the large intensity region is distributed in the south-north direction near the Chelungpu fault and close to epicenter regions. The largest intensity was recorded at TCU084 (hanging wall) station as a 6+ in the JMA scale in the east side of epicenter, following the same intensity level by TCU052 (hanging wall), TCU068 (hanging wall) both in the northern part of the fault, and TCU065 (foot wall) in the central part of the fault stations.

The relation between seismic intensity and larger of the two horizontal acceleration (PGA_h) is given in Equation (2.2.1) for the 420 Chi-Chi event records.

$$I_{JMA} = 1.04 + 1.78 \log_{10}(PGA)_h \qquad \sigma = 0.188 \qquad (2.2.1)$$

Figure 2.2.4 compares the obtained relation with the relation of Tong and Yamazaki (1996), which was derived using 205 sets of accelerograms obtained from earthquakes in Japan (1993 Kushiro-Oki EQ, 1994 Hokkaido-Nansei-Oki EQ, 1994 Hokkaido-Toho-Oki EQ, 1994 Sanriku-Haruka-Oki EQ, 1995 Hyogoken-Nanbu EQ and its aftershock) and in California (1994 Northridge EQ). Some difference is observed between the two PGA-JMA intensity relations. Since the long period contents are dominant in some records in the Chi-Chi event, the same PGA value gives a larger intensity.

Spectrum Intensity

The spectrum intensity (*SI*) is one of the ground motion indices that is used to estimate the structural damage due to earthquake. In Japan, the SI value is used as the index to shut-off natural gas supply after a damaging earthquake. Based on the seismic records and damage of gas pipes around the instruments due to the 1995 Kobe earthquake, a SI value of 60cm/s was set as the level of shaking to mandatorily shut-off a city gas supply. In this objective, Tokyo Gas Co., Ltd. has developed the SI sensor (Katayama et al., 1998) and the new SI sensor (Shimizu et al., 2000), which calculate the SI value in the sensor using horizontal acceleration records. Recently, the deployment of new SI-sensors has started in Tokyo metropolitan area, and the super dense seismic monitoring system (SUPREME) with 3,700 new SI sensors will be completed by 2007.

The spectrum intensity is calculated as the area under the relative-velocity response spectrum with damping ratio 0.2 between the periods of 0.1 s and 2.5 s, divided by the period interval (Figure 2.2.5). In this study the SI values are computed for each 1.0 degree on the horizontal plane and the maximum of them is defined as the SI. Equation (2.2.2) is the relationship between the I_{JMA} and *SI*, calculated for the 420 Chi-Chi event records.

$$I_{JMA} = 2.23 + 1.94 \log_{10} SI \qquad \sigma = 0.112 \qquad (2.2.2)$$

Figure 2.2.6 shows the comparison between the obtained relationship for the Chi-Chi earthquake and the relationship proposed by Tong and Yamazaki (1996). The SI-JMA intensity relation for the Chi-Chi earthquake is almost same as the existing relation. This observation indicates that both the JMA intensity and SI are not affected by long period contents, which are dominant in the records such as TCU068 and TCU052.

The relationship between the SI and PGV is shown in Figure 2.2.7 for the 420 records of the Chi-Chi earthquake. Although, in most cases the SI value is very close to the PGV (SI=1.18 PGV by Tong and Yamazaki, 1995), a large difference is observed for some near-fault stations (e.g. TCU068, TCU052). This observation can be explained by the fact that the long period contents larger than 2.5 s are dominant in these records. Since the SI is obtained as the average amplitude of the velocity response between 0.1 s and 2.5 s, it is not reflect such long period contents. On the contrary, the PGV is affected by such long period contents, as seen in the plots of the velocity response spectra in the following section. The PGV reached as much as 384 cm/s in TCU068, due to the long period pulse motion, while the SI and JMA intensity are 82 cm/s and 6.1, respectively. Hence we must be careful to use PGV as an index to estimate structural damage.

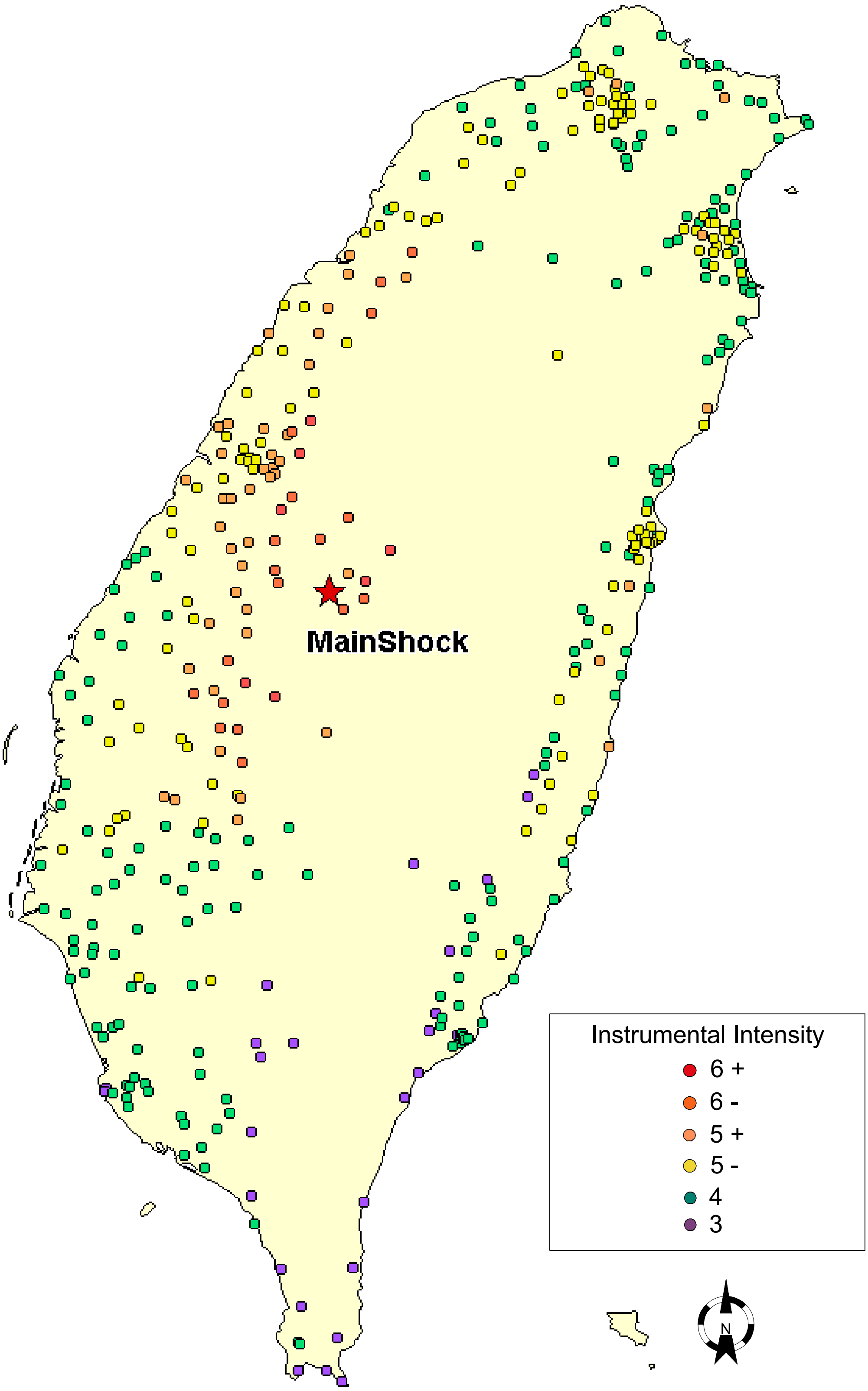

Figure 2.2.3. Distribution of the JMA seismic intensity for the 1999 Chi-Chi earthquake (Refer to color figure 1).

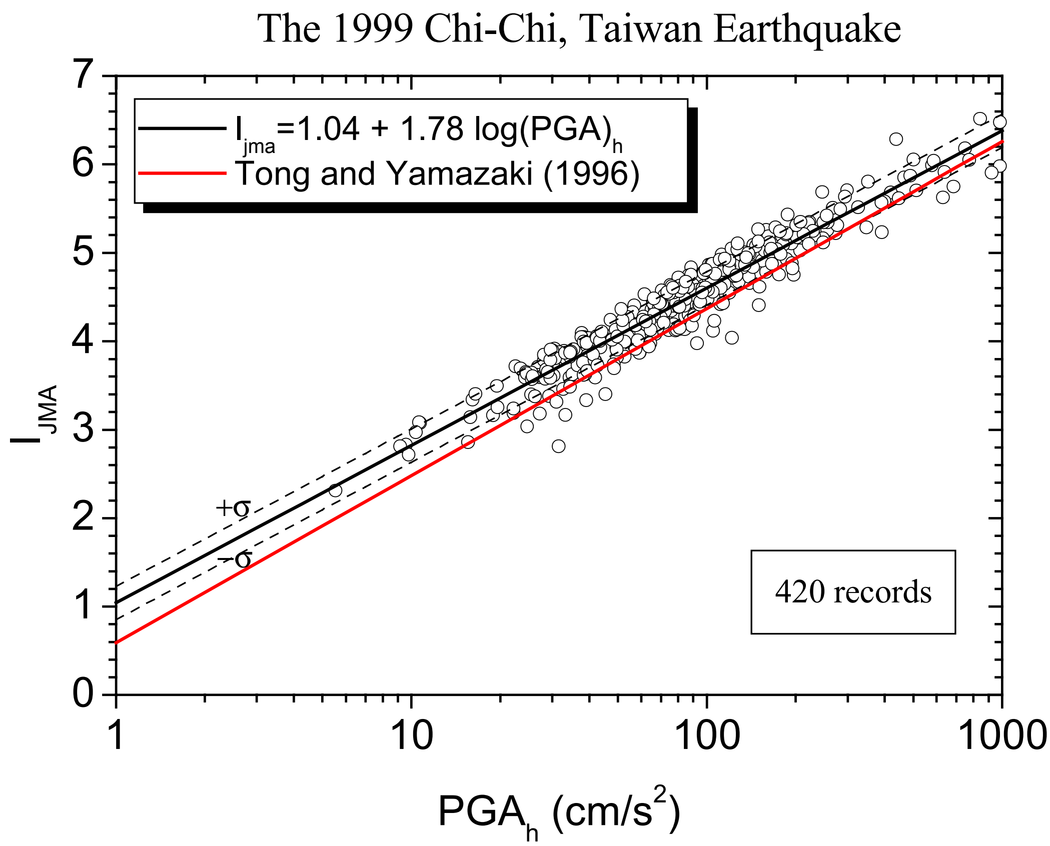

Figure 2.2.4. Comparison of the relation between seismic intensity (I_{JMA}) and larger of two horizontal PGAs with the relation of Tong and Yamazaki (1996).

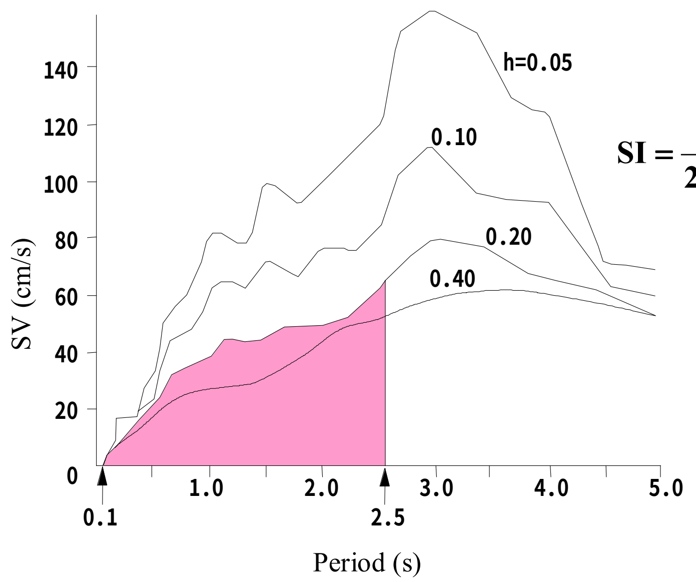

$$SI = \frac{1}{2.4}\int_{0.1}^{2.5} SvdT(h = 0.2)$$

Figure 2.2.5. Definition of Spectrum Intensity SI.

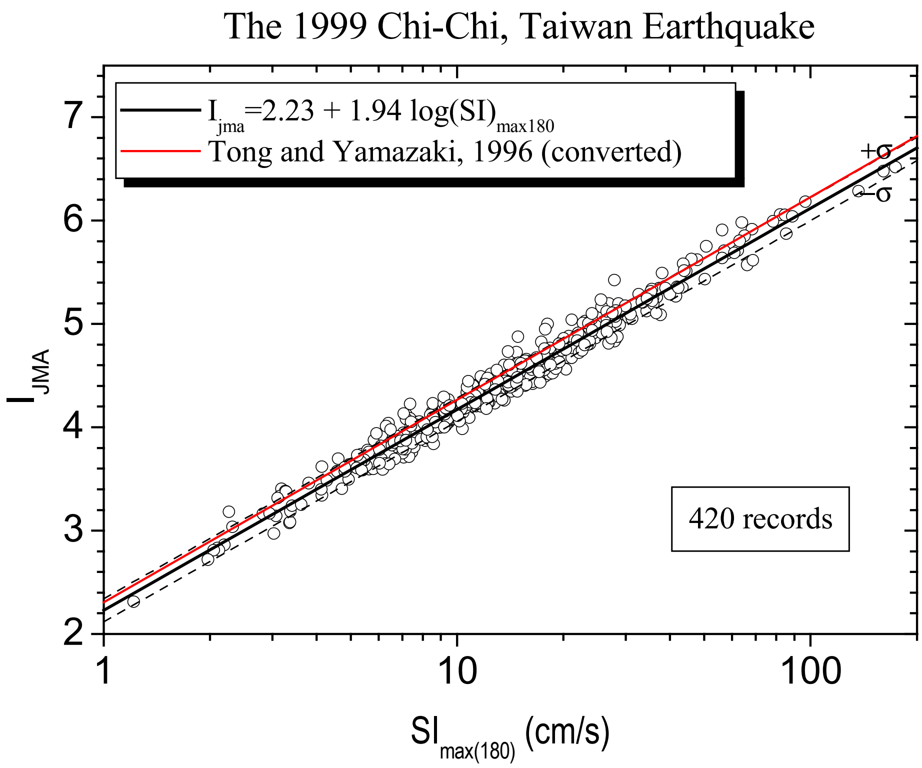

Figure 2.2.6. Relationship between the I_{JMA} and SI, calculated for the Chi-Chi earthquake, and that proposed by Tong and Yamazaki (1996).

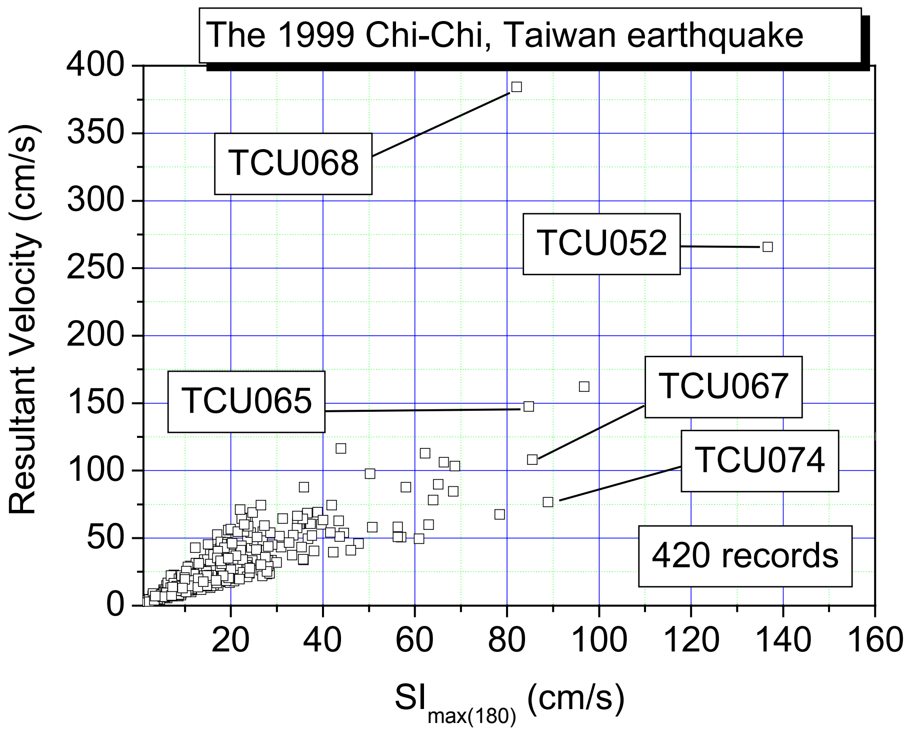

Figure 2.2.7. Resultant peak ground velocity with respect to the spectral intensity for 420 stations from the 1999 Chi-Chi earthquake.

2.2.3 Near Fault Strong Motion

Maximal Ground Motion

In order to demonstrate the characteristics of near-fault strong motion from the large crustal earthquake, the resultant velocity time histories of two horizontal components on the horizontal plane between 0^0-360^0 are calculated for sixteen near-fault stations.

To examine the effects of the hanging wall and footwall, and those of the forward and backward rupture propagations from the hypocenter, the location of some near-fault stations and their maximal velocity directions are demonstrated along the surface fault in Figure 2.2.8. In the figure, the arrow bars indicate the maximal velocity direction on the horizontal plane. The difference in the amplitudes of strike-normal and strike-parallel components is very important characteristics of the near-fault ground motion records (Somerville et al., 1997; Somerville, 2000). The PGV is observed to be much larger on the hanging wall side (TCU 068, TCU052) than the footwall side (TCU065, TCU067). The maximum velocity direction is observed as normal to the fault for both the hanging wall stations (TCU068 and TCU072) and footwall stations (TCU0129, TCU076, TCU075, TCU065, TCU067, and TCU054), but their directions are opposite.

Figure 2.2.9 shows the fault-slip distribution and the snapshot moment release process for the Chi-Chi, Taiwan earthquake by Yagi and Kikuchi (1999). We compare the orientation of the maximal velocity direction (due to wave propagation from the hypocenter to the stations) and the actual (known) orientation of slip and the slip velocity (moment release process) on the fault. The northwest maximal velocity directions are observed at the TCU074, TCU078, and TCU089 stations in Figure 2.2.8. This dominant velocity direction (northwest) can be seen in the Figure 2.2.9, from the starting point of the rupture propagation up to 15s. The maximum slip velocity reaches to 0.9 m/s on about 20s after the rupture propagation start (in the north and northwest of the epicenter, Figure 2.2.9).

Figures 2.2.10 to 2.2.12 show the orientation of maximal velocity directions on the horizontal plane, the velocity and acceleration time histories in the maximal velocity direction, respectively. The forward directivity effect, which causes most of the seismic energy from the rupture in a single large pulse-like motion at the beginning of the records, can be clearly observed at TCU052, TCU068, TCU075, TCU076, and TCU102 stations located very near the Chelungpu fault

Characteristics of Response Spectra

To investigate the damage potential in terms of frequency contents for those importance records, the acceleration and velocity response spectra with 0.05 damping for the two horizontal components and the maximal velocity direction were calculated.

Figures 2.2.13 and 2.2.14 show the predominant period of the acceleration and velocity response spectra to the maximal velocity direction for the sixteen near-fault stations. From these figures, the effect of the pulse motion is clearly seen in the velocity response spectra. The predominant period becomes longer as the stations go to the north along the fault (corresponding the rupture propagation): about 1-2s for TCU076 and TCU129, about 4-5s for TCU075 and TCU065, and about 10s for TCU052 and TCU068. The period of the pulse became longer by the cumulative effect of the seismic radiation from the fault (Somerville, 2000).

Figures 2.2.15 and 2.2.16 show the acceleration response spectra and velocity response spectra of the two horizontal components and the maximal direction for the sixteen selected near-fault stations. In these figures, the change of amplitudes and spectral shape due to the forward directivity effect is clearly observed.

It is an important lesson from the Chi-Chi earthquake that the near fault motion is quite intense and dependent on the location with respect to the fault. The location of the hypocenter (the start point of the rupture) and the direction of rupture propagation strongly affect the intensity and spectral contents observed, even the range of the rupture is same. However, these parameters are difficult to predict before an earthquake. Even though, if an active fault is known, we can design important structures considering the fault-normal and fault-parallel directions.

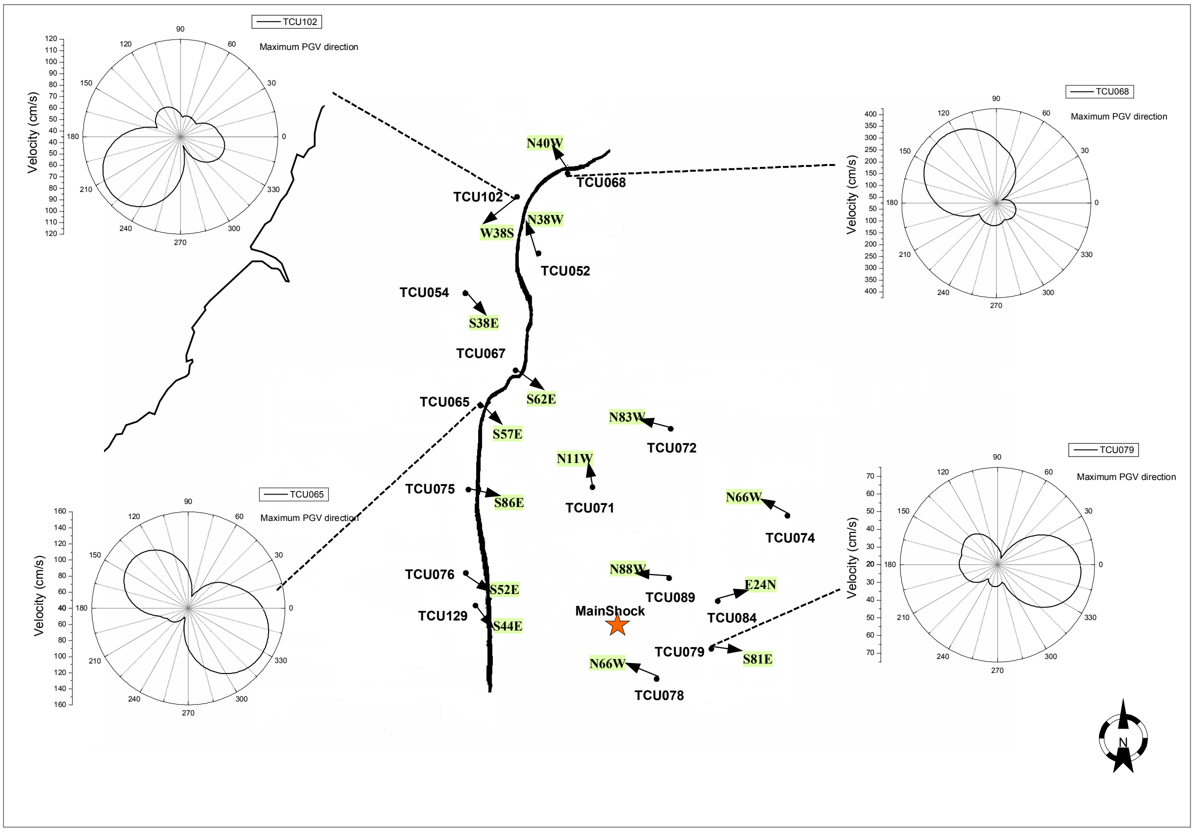

Figure 2.2.8. Locations of the sixteen near-fault stations, corresponding maximal velocity direction (arrow bar) for each near-fault station, and rotated maximum PGV direction for some stations.

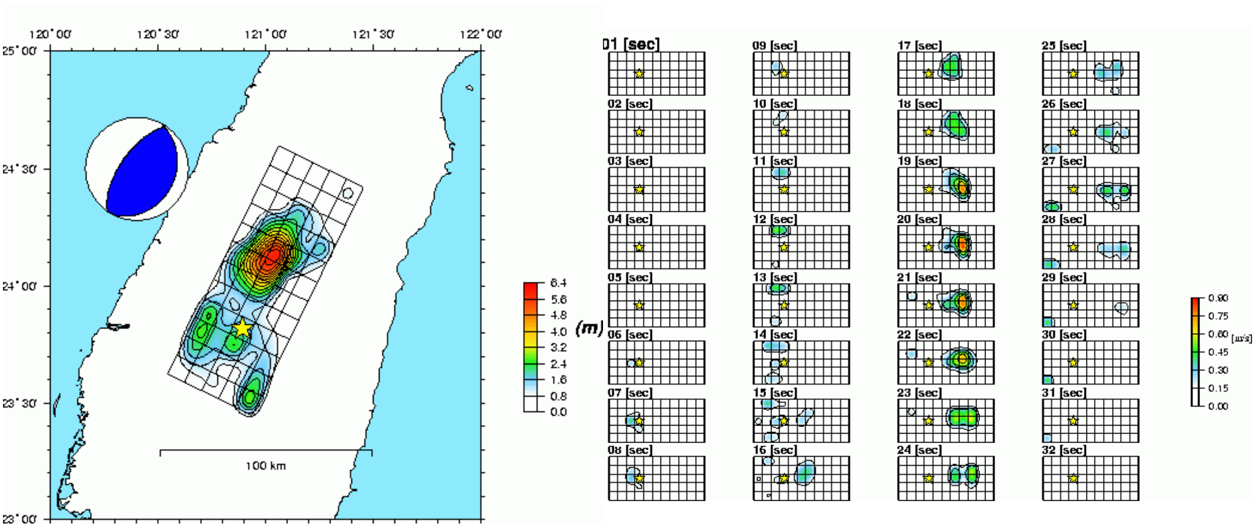

Figure 2.2.9. Distribution of the fault-slip for the 1999 Chi-Chi, Taiwan earthquake and snap shot of moment release process by Yagi and Kikuchi (1999).

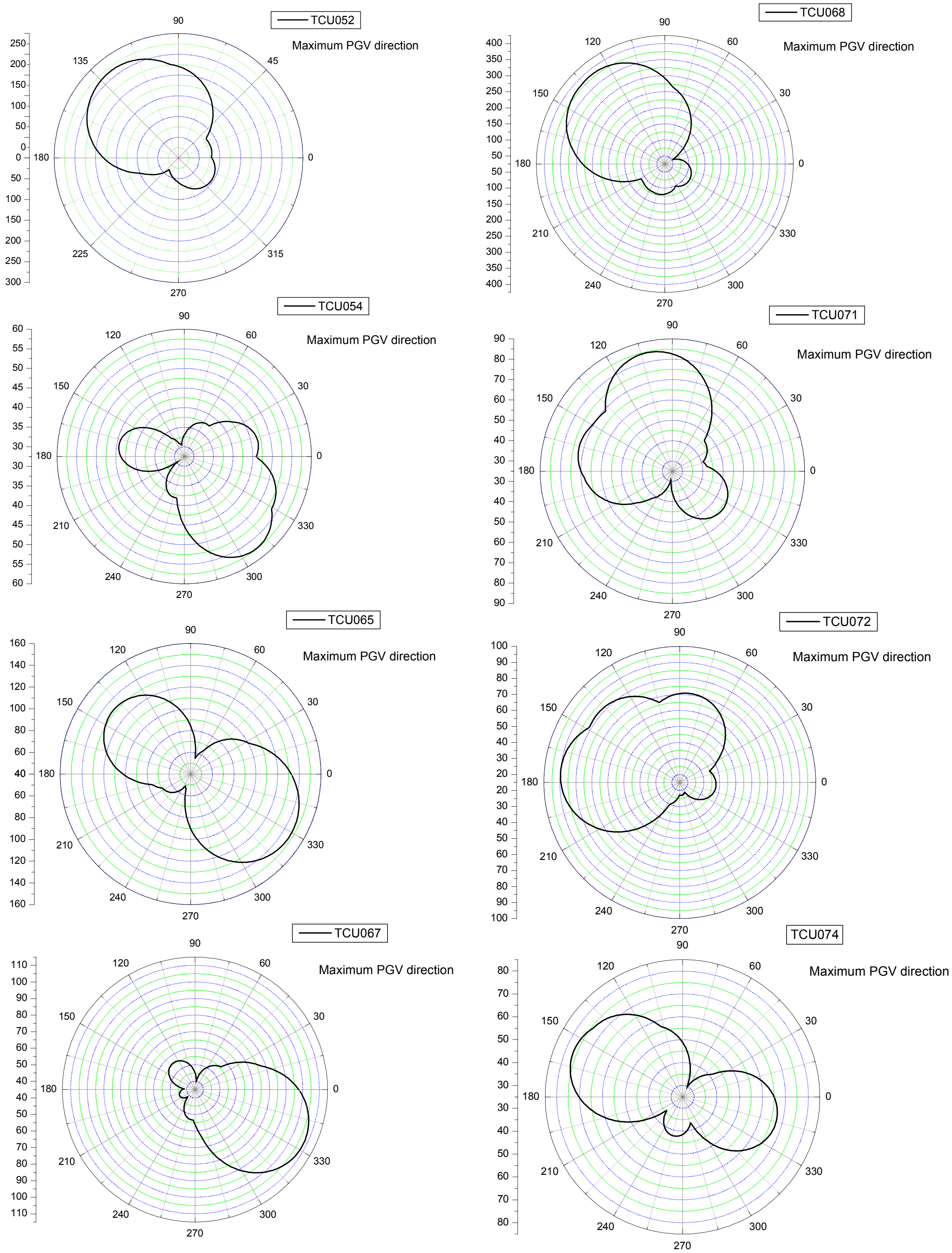

Figure 2.2.10. Maximal velocity direction on the horizontal plane for the sixteen near-fault stations.

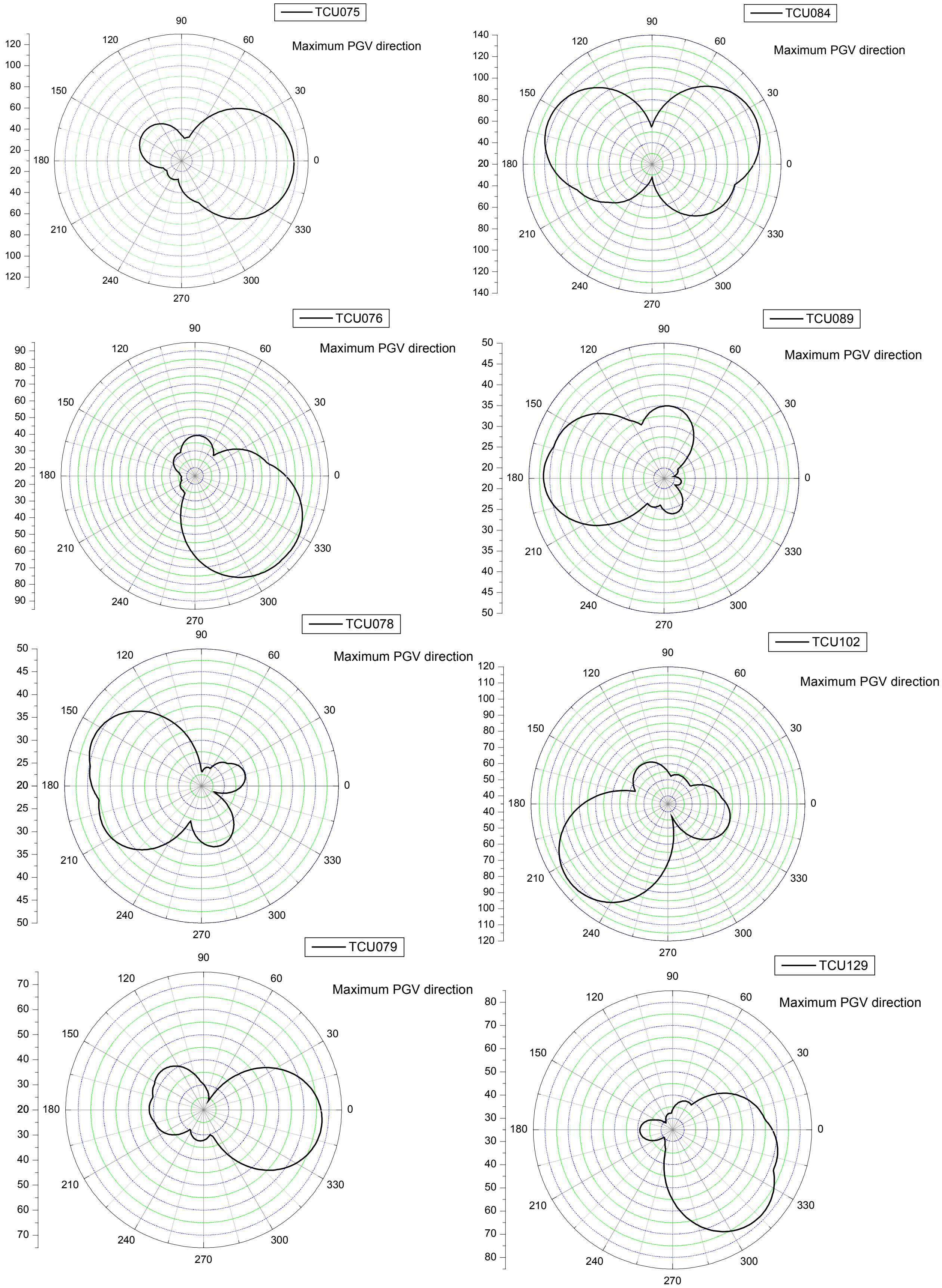

Figure 2.2.10. Maximal velocity direction on the horizontal plane for the sixteen near-fault stations (Continued).

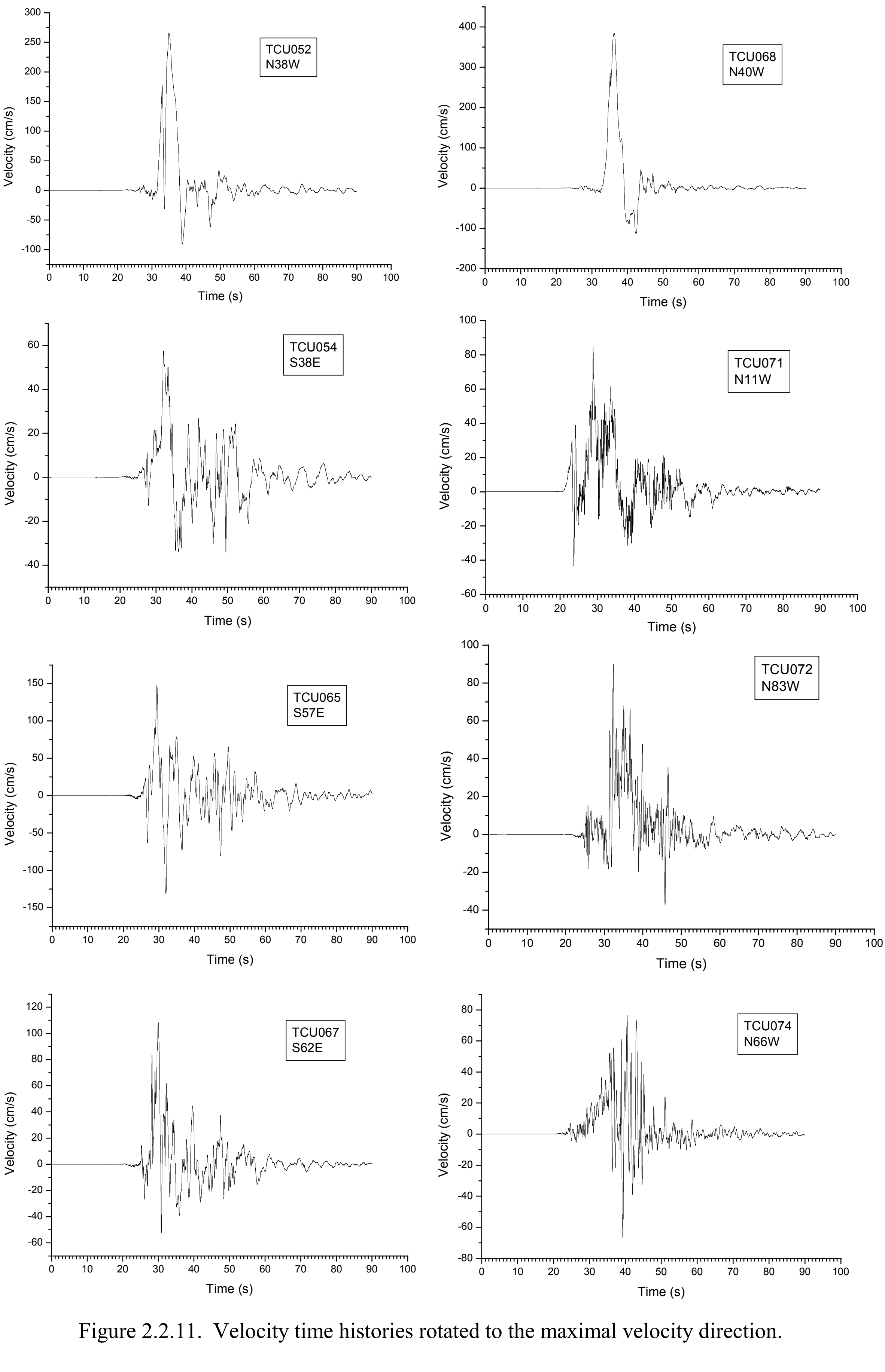

Figure 2.2.11. Velocity time histories rotated to the maximal velocity direction.

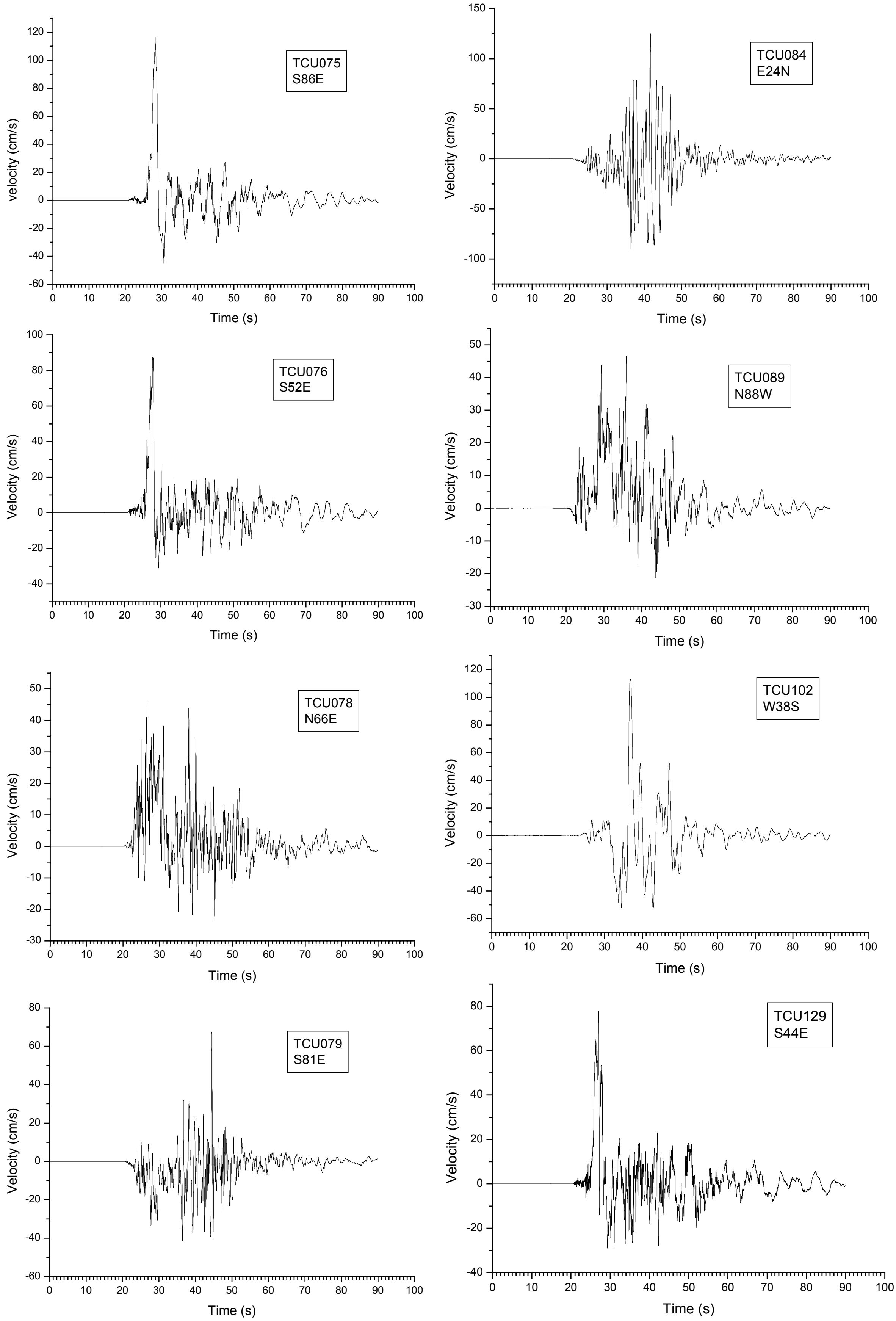

Figure 2.2.11. Velocity time histories rotated to the maximal velocity direction (Continued).

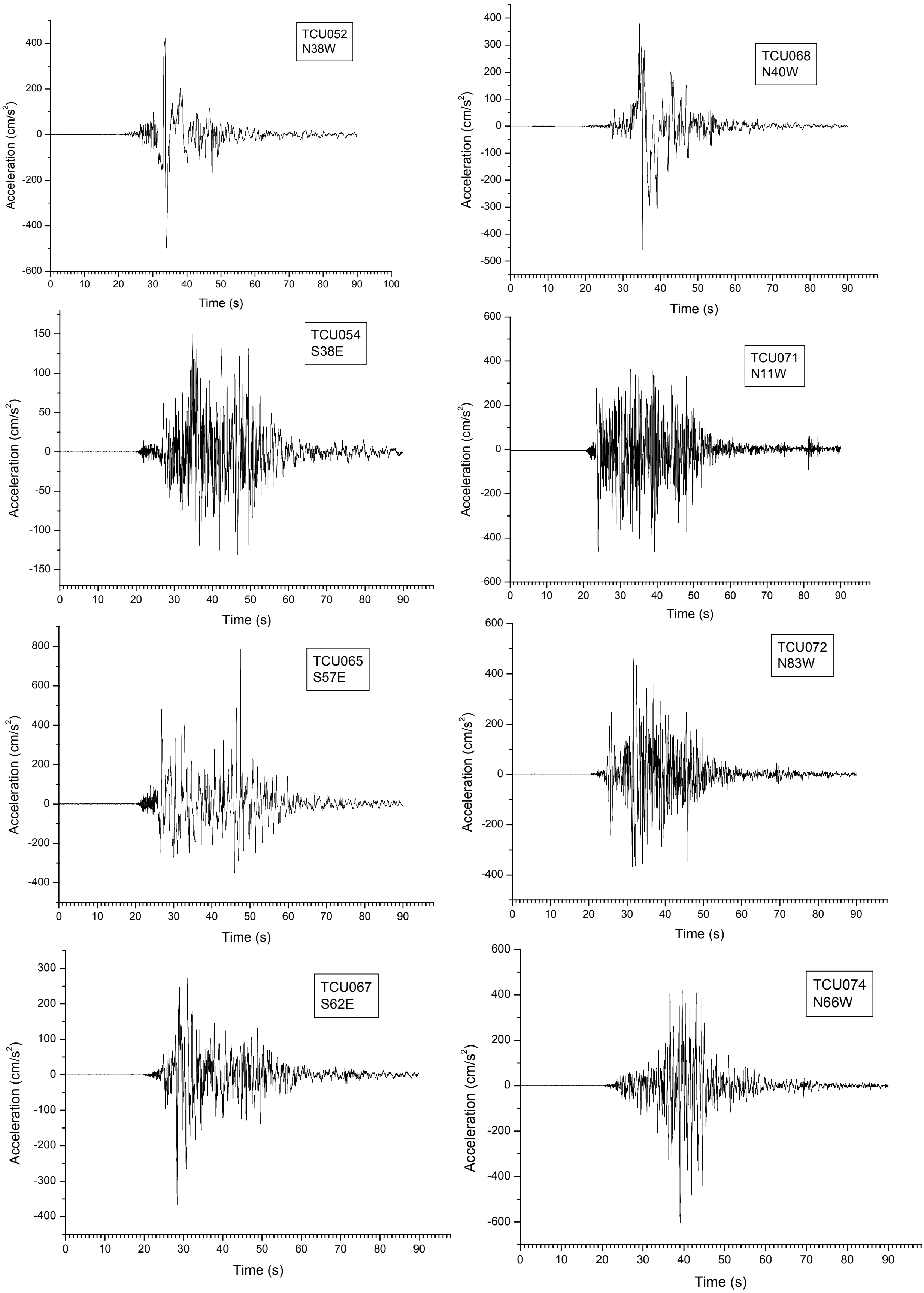

Figure 2.2.12. Acceleration time histories rotated to the maximal velocity direction.

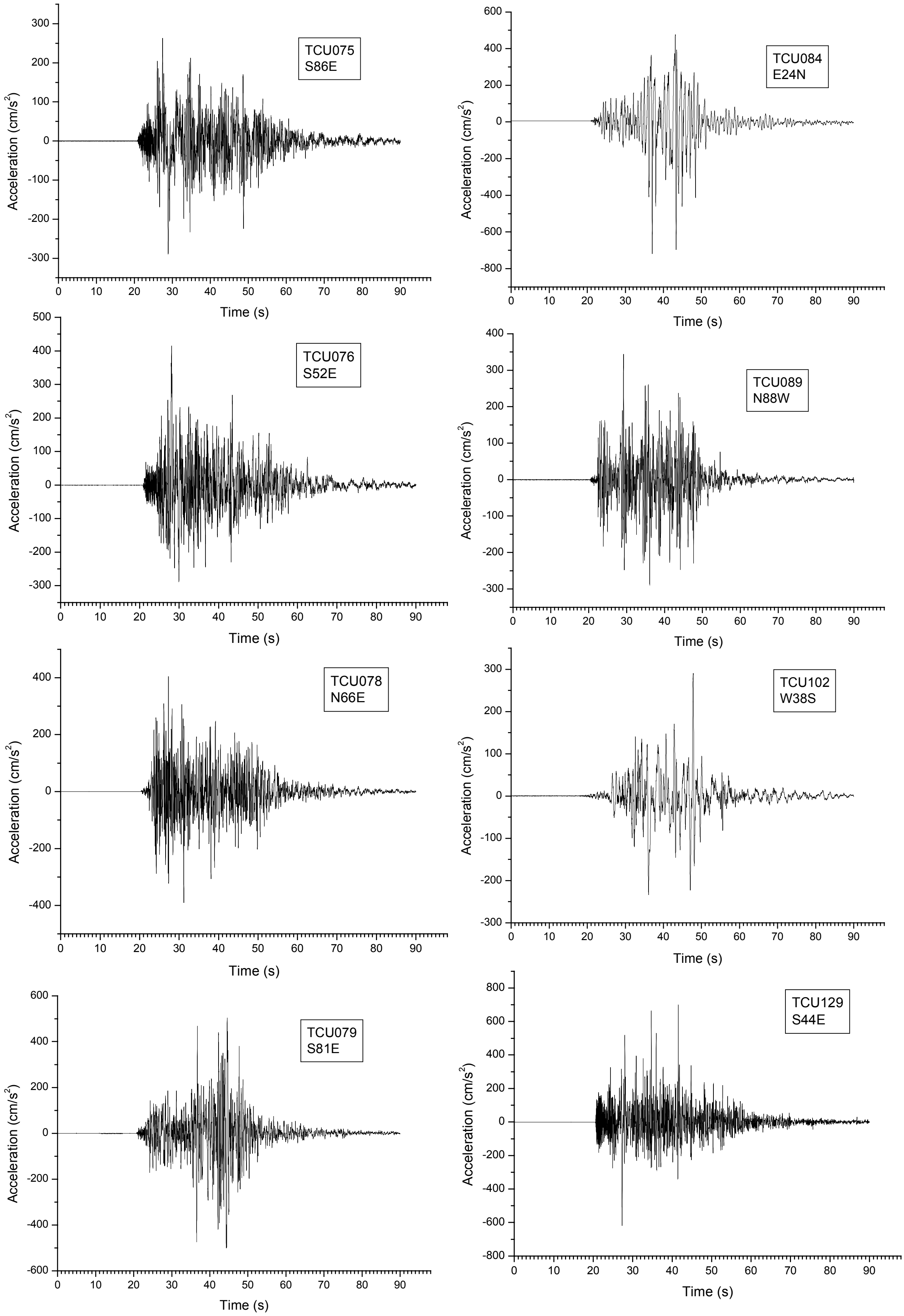

Figure 2.2.12. Acceleration time histories rotated to the maximal velocity direction (Continued).

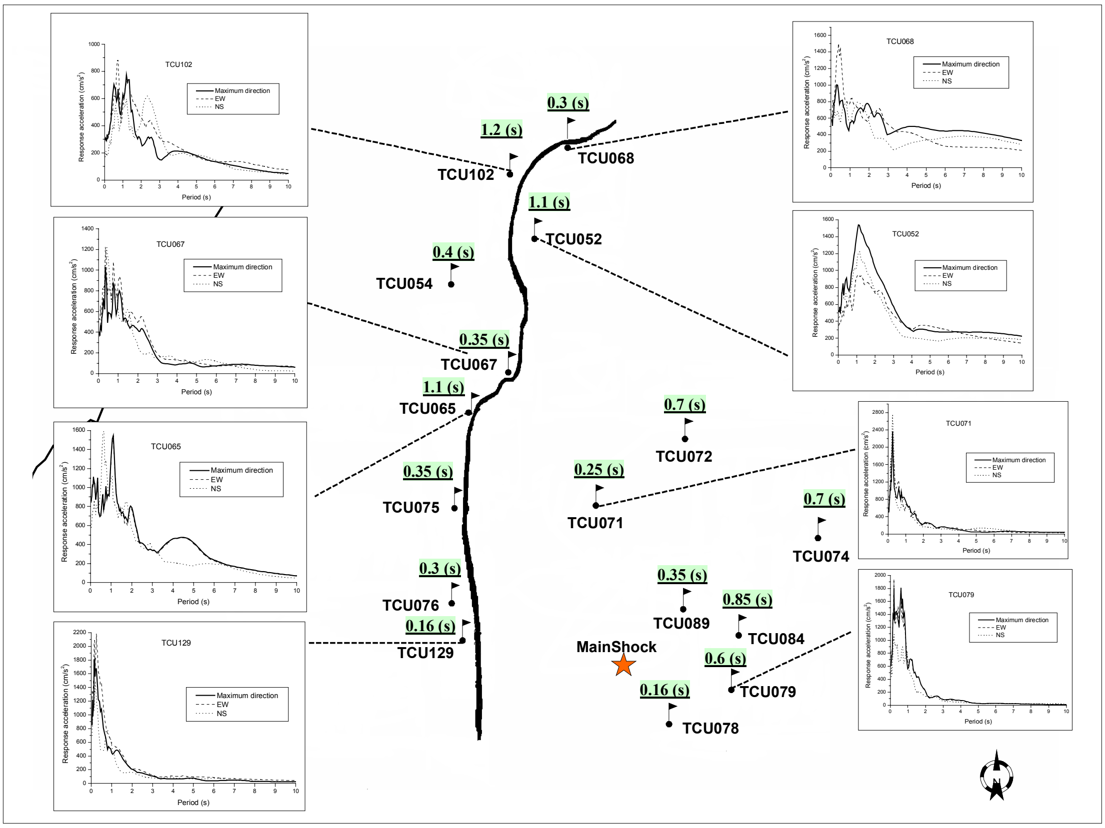

Figure 2.2.13. Distribution of the predominant period for the sixteen near-fault stations and the acceleration response spectra for these stations.

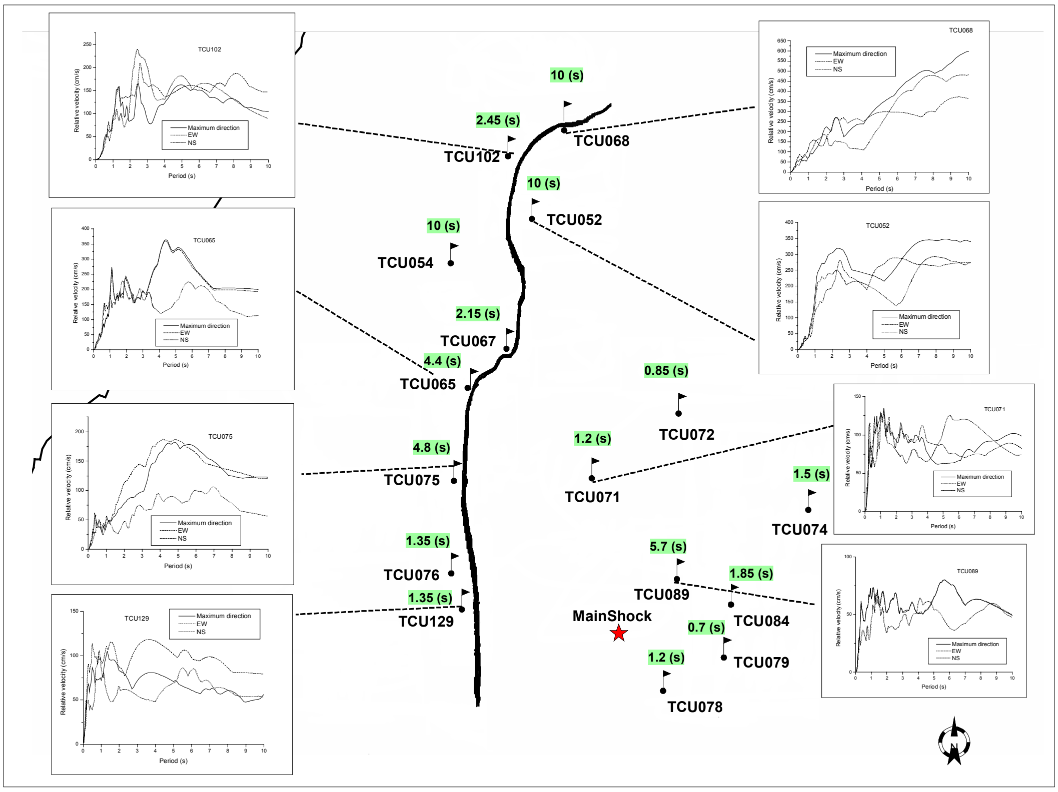

Figure 2.2.14. Distribution of the predominant period for the sixteen near-fault stations and the velocity response spectra for these stations.

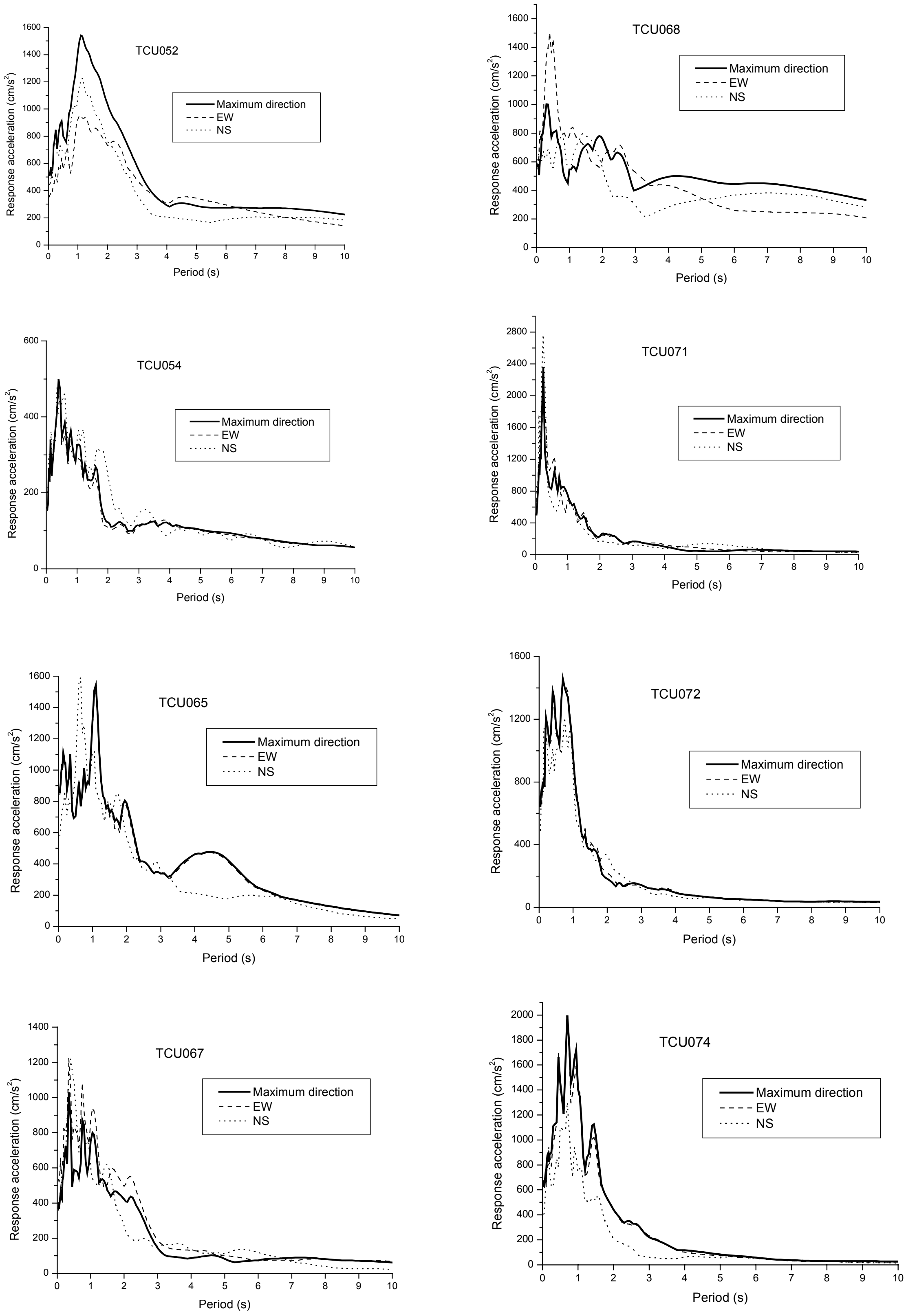

Figure 2.2.15. The acceleration response spectra of two horizontal components and the maximum velocity direction with 0.05 damping for the sixteen near-fault stations.

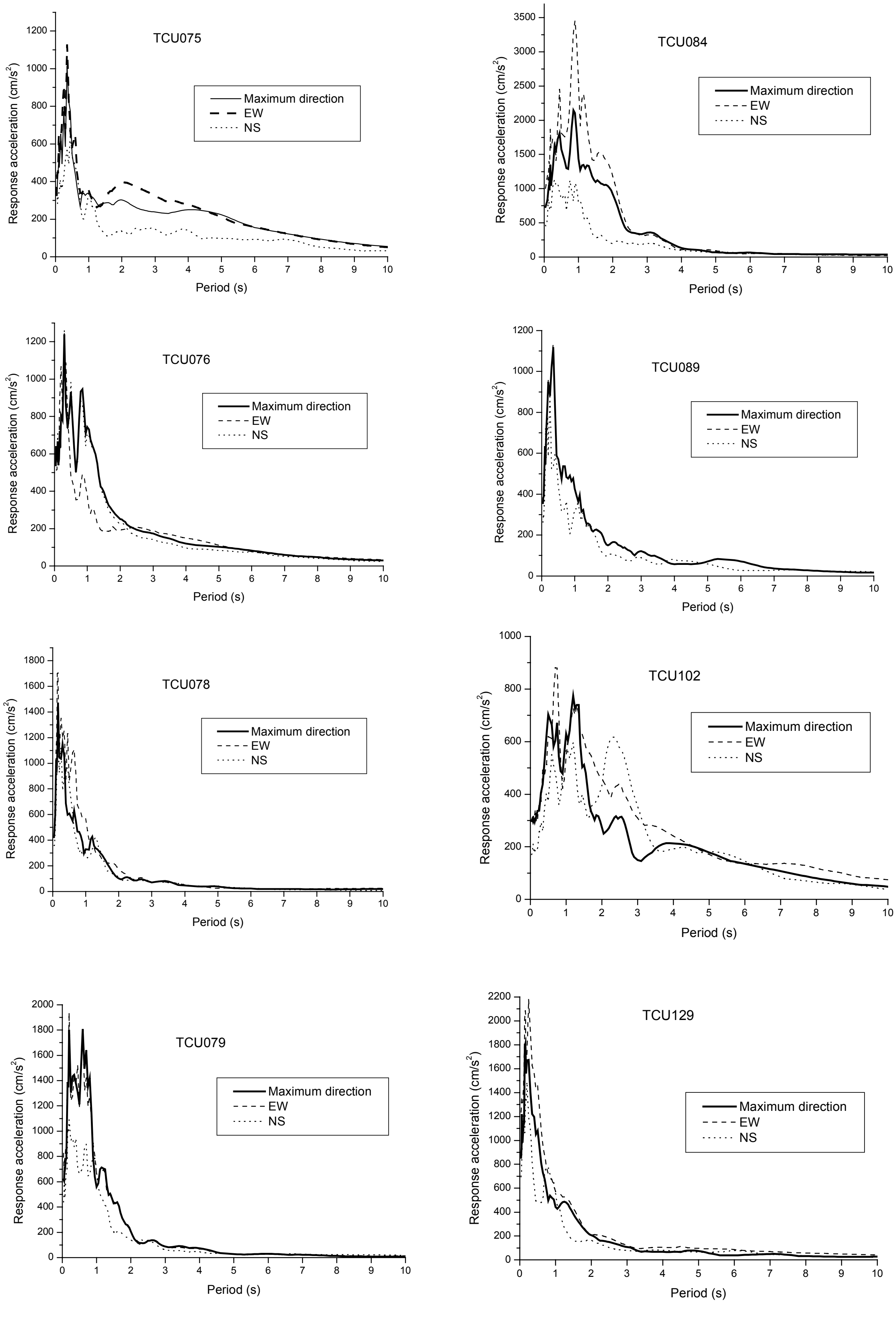

Figure 2.2.15. The acceleration response spectra of two horizontal components and the maximum velocity direction with 0.05 damping for the sixteen near-fault stations (Continued).

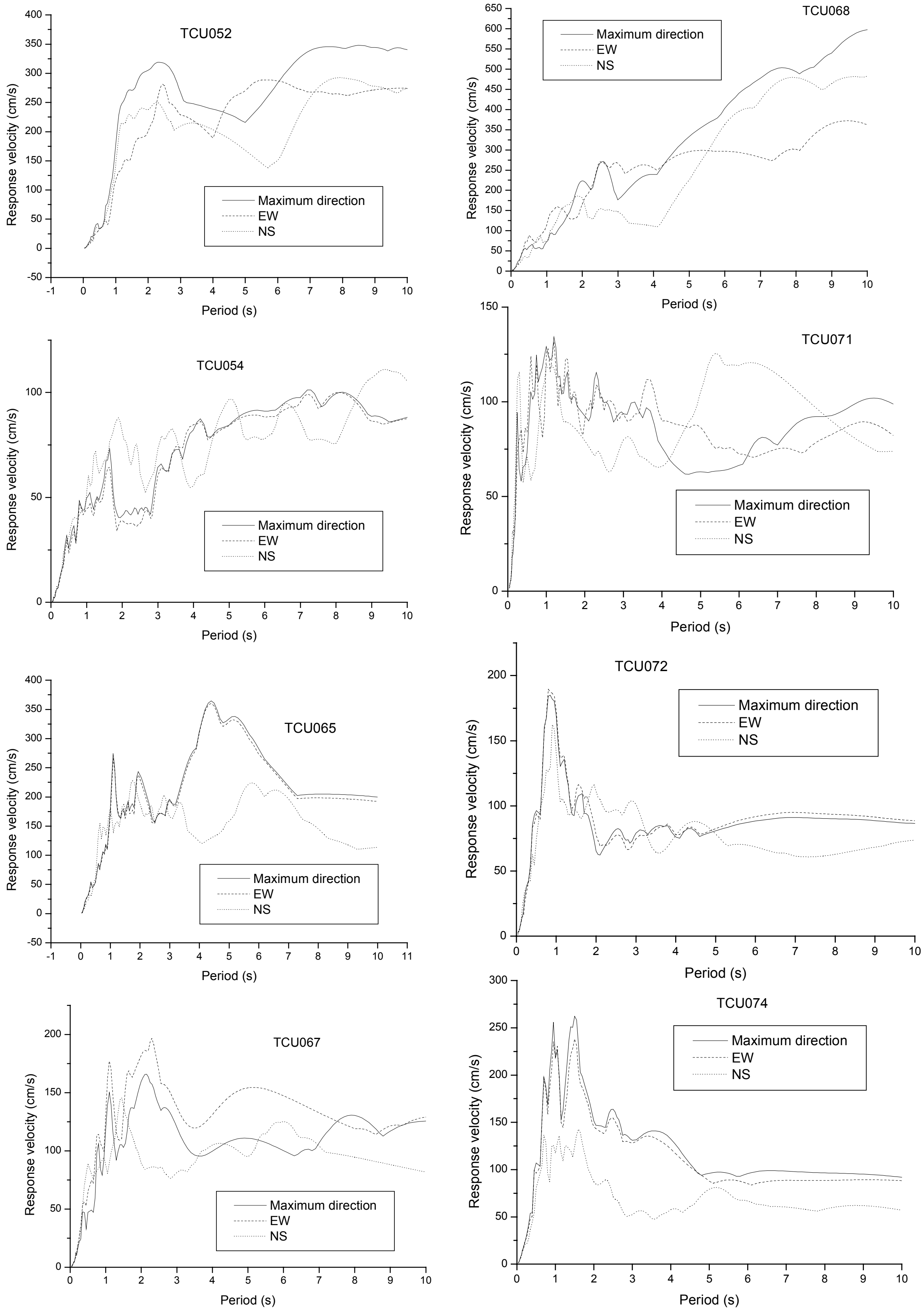

Figure 2.2.16. The velocity response spectra of two horizontal components and the maximum velocity direction with 0.05 damping for the sixteen near-fault stations.

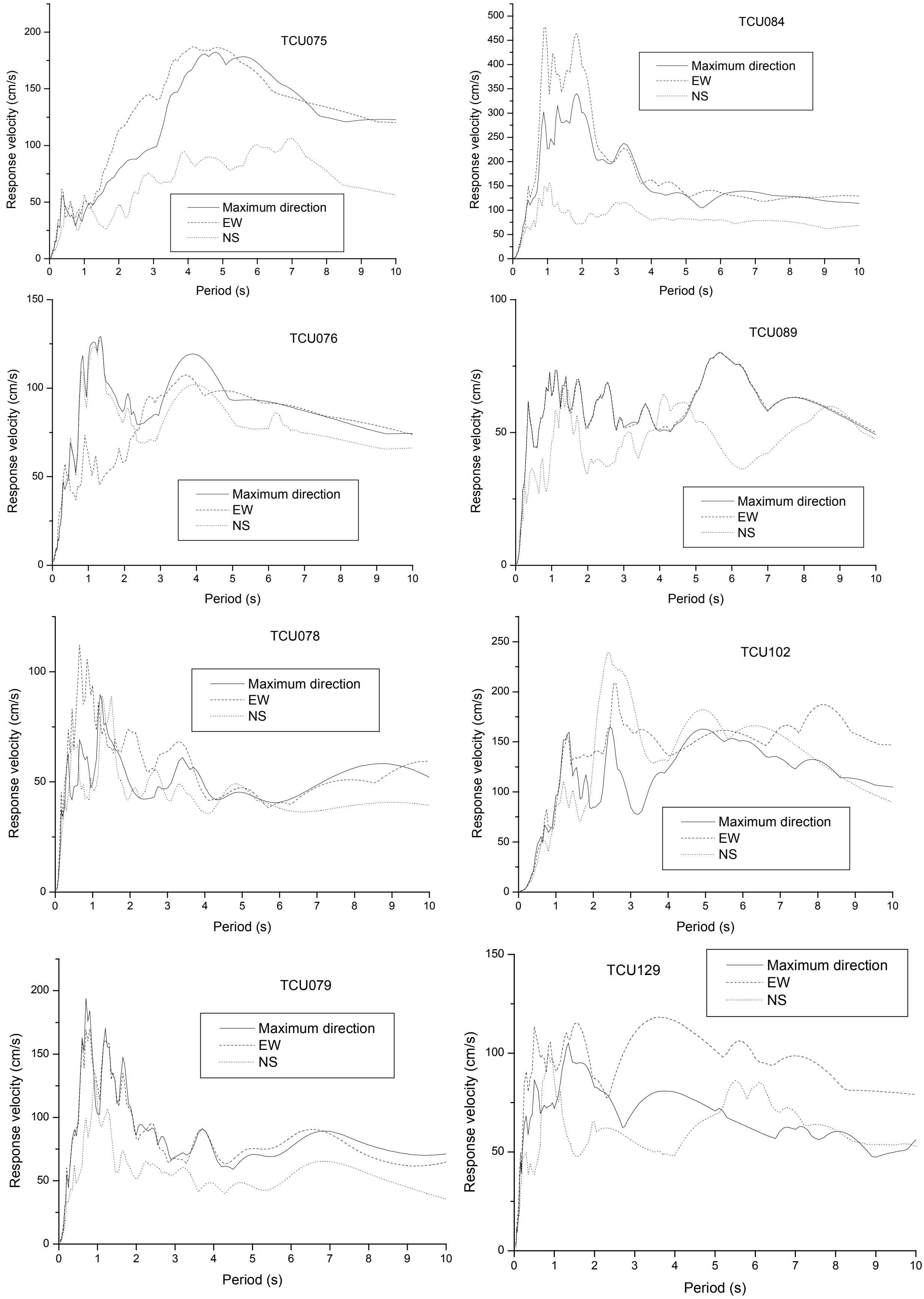

Figure 2.2.16. The velocity response spectra of two horizontal components and the maximum velocity direction with 0.05 damping for the sixteen near-fault stations (Continued).

2.2.4 Summary

The characteristics of the free-field strong ground motion records of the 1999 Chi-Chi, Taiwan earthquake were investigated. Using 420 three-component records of the world densest network of Seismological Center of Central Weather Bureau of Taiwan, the strong motion indices such as *PGA*, *PGV*, I_{JMA}, and *SI* were calculated (listed in Appendix). At the stations near the Chelungpu fault with 100 kilometers south-north extension, a large pulse-like motion with the period longer than 3 seconds was observed in the velocity time histories to the direction of maximum amplitude. This pulse–like motion represents the cumulative effect of the seismic radiation from the fault rupture toward the sites.

At TCU052 and TCU068 stations in the northeast hanging-wall side of Chelungpu fault, the PGV reached as large as 266cm/s and 384cm/s, respectively. In spite of these large PGV values, structural damages around the instruments were not so severe. This is due to the fact that the period of the pulse is too long at these stations. Since the PGV is affected by such a long period content, it is sometimes not a reliable parameter to express structure damages. In this sense, the I_{JMA} and *SI* values reflected the damage status more than PGV did in the Chi-Chi earthquake.

To investigate the characteristics of near-fault ground motion records in terms of spectral contents, the acceleration and velocity response spectra to the maximal velocity direction were calculated for sixteen near-fault stations. From the preliminary analysis results, the forward rupture directivity was clearly observed in the northern part of Chelungpu fault. A large pulse motion with period longer than 5 seconds was observed to the direction almost normal to the fault. This directivity pulse may give significant effects to long period structures. Fortunately, however, there were no such long period structures along the Chelungpu fault when the earthquake occurred.

Since the 1999 Taiwan earthquake provided reliable strong ground motion data, especially for near-fault records, a future study is necessary considering source parameters such as the direction of slip on the fault and its slip rate and the site and geological conditions as well as forward rupture directivity effects.

References

Boore, D.M. (1999). “Effect of baseline corrections on response spectra for two recordings of the 1999 Chi-Chi, Taiwan, earthquake,” *U.S. Geological Survey Open-file Report,* No.99-545.

Japan Meteorological Agency (JMA) Report (1996). “Note on the JMA seismic intensity,” *Gyosei*, (in Japanese).

Katayama T. N. Sato, and K. Saito (1988). “SI-sensor for the Identification of Destructive Earthquake Ground Motion,” *Proc. of the 9th World Conference on Earthquake Engineering*, VII, pp. 667-672.

Kostadinov, M and F. Yamazaki (2000). “Destructiveness of near-fault ground motion from the 1999 Chi-Ch-, Taiwan earthquake,” *The 55th Annual Conference of JSCE*, (in press).

Lee W.H.K., T.C. Shin, K.W. Kuo, and K.C. Chen (1999). “Free-field strong ground motion data from the 9/21 Chi-Chi earthquake,” *Digital acceleration files on CD-ROM, Vol.1*, Seismological Center, Central Weather Bureau, Taipei, Taiwan.

Loh C.H., Z.K. Lee, T.C. Wu, and S.Y. Peng (2000). “Ground Motion Characteristics of the Chi-Chi earthquake of September 21, 1999,” *Earthquake Engineering and Structural Dynamics*, Vol. 29, No. 6, 867-897.

Shabestari T.K and F. Yamazaki (1998). “Attenuation relationship of JMA seismic intensity using JMA records,” *Proceedings of the 10th Japan Earthquake Engineering Symposium*, Vol.1, 529-534.

Shin T.C., K.W. Kuo, W.H.K. Lee, T.L. Teng, and Y.B.Tsai (2000). “A preliminary report on the 1999 Chi-Chi (Taiwan) earthquake,” *Seismological Research Letters*, Vol.71, No.1.

Shimizu Y., A Watanabe, K. Koganemaru, W. Nakayama, and F. Yamazaki (2000). "Super High-Density Realtime Disaster Mitigation System," *12th World Conference on Earthquake Engineering,* CD-ROM, 7p.

Somerville P., Smith N.F., Graves R.W., and Abrahamson N.A. (1997). "Modification of empirical strong ground motion attenuation relations to include the amplitude and duration effects of rupture directivity," *Seismological Research Letters*, 68 (1), 199-222.

Somerville P. (2000). "Characterized of near fault ground motions," *U.S.-Japan Workshop: Effects of Near-Field Earthquake Shaking*, PEER and ATC.

Tong H. and F. Yamazaki (1995). "A Relationship Between Seismic Ground Motion Severity and House Damage Ratio," *Proc. of 4th U.S. Conference on Lifeline Earthquake Engineering,* ASCE, 33-40.

Tong H. and F. Yamazaki (1996). "Relationship between ground motion indices and new JMA seismic intensity," *Seisan-kenkyu*, Vol.48, No.11 (in Japanese).

Yagi, Y. and M. Kikuchi (1999). "Distribution of source rupture process for Taiwan earthquake," *Open-file report on Special event Taiwan Earthquake*, Earthquake Research Institute, Tokyo University.

Yamazaki F. (1998). "Real-time earthquake disaster mitigation system in Japan," *Seismology and earthquake engineering in Japan,* Property and Casualty Insurance Rating Organization of Japan, 133-149, Japan.